HHS Public Access

Author manuscript

Biol Psychiatry. Author manuscript; available in PMC 2022 December 01.

Published in final edited form as:

Biol Psychiatry. 2021 December 01; 90(11): 742–755. doi:10.1016/j.biopsych.2021.05.027.

Developmental and behavioral phenotypes in a mouse model of DDX3X syndrome

Andrea Boitnott[1,2,3,4,*], **Marta Garcia-Forn**[1,2,3,4,*], **Dévina C Ung**[1,2,3,4], **Kristi Niblo**[1,2,3,4], **Danielle Mendonca**[1,2,3,4], **Yeaji Park**[1,2,3,4], **Michael Flores**[1,2,3,4,5], **Sylvia Maxwell**[1,2,3,4,6], **Jacob Ellegood**[7], **Lily R Qiu**[8], **Dorothy E Grice**[1,2], **Jason P Lerch**[7,8,9], **Mladen-Roko Rasin**[10], **Joseph D Buxbaum**[1,2,3,4,11], **Elodie Drapeau**[1,2], **Silvia De Rubeis**[1,2,3,4]

[1]Seaver Autism Center for Research and Treatment, Icahn School of Medicine at Mount Sinai, New York, NY 10029, USA.

[2]Department of Psychiatry, Icahn School of Medicine at Mount Sinai, New York, NY 10029, USA.

[3]The Mindich Child Health and Development Institute, Icahn School of Medicine at Mount Sinai, New York, NY 10029, USA.

[4]Friedman Brain Institute, Icahn School of Medicine at Mount Sinai, New York, NY 10029, USA.

[5]Department of Biology, New York University, College of Arts and Science, New York, NY 10003, USA.

[6]The Bronx High School of Science, NY 10468, USA

[7]Mouse Imaging Centre, Hospital for Sick Children, Toronto, Ontario, ON M5T 3H7, Canada.

[8]Wellcome Centre for Integrative Neuroimaging, FMRIB, Nuffield Department of Clinical Neuroscience, University of Oxford, Oxford, OX3 9DU, UK.

[9]Department of Medical Biophysics, University of Toronto, Toronto, Ontario, ON M5T 3H7, Canada.

[10]Department of Neuroscience and Cell Biology, Rutgers University, Robert Wood Johnson Medical School, Piscataway, NJ 08854, USA

[11]Department of Neuroscience, Icahn School of Medicine at Mount Sinai, New York, NY 10029, USA.

Abstract

[§]Correspondence: silvia.derubeis@mssm.edu (S.D.R).

[*]These authors contributed equally to this work

Conceptualization: SDR, AB, DCU, MGF, ED; Investigation: SDR, AB, DCU, MGF, KN, DM, YP, MF, SM, JE, LRQ; Formal analyses: SDR, AB, DCU, MGF, JE; Writing-original draft: SDR, AB, DCU, MGF; Writing – review and editing: SDR, AB, DCU, MGF, KN, DM, YP, MF, SM, DEG, MRR, JDB, ED, JE, LRQ, JPL; Funding acquisition: SDR, JDB; Resources: SDR, MRR, JDB; DEG provided expertise on relationship to clinical phenotype.

The authors report no biomedical financial interests or potential conflicts of interest.

Background: Mutations in the X-linked gene *DDX3X* account for ~2% of intellectual disability in females, often co-morbid with behavioral problems, motor deficits, and brain malformations. *DDX3X* encodes an RNA helicase with emerging functions in corticogenesis and synaptogenesis.

Methods: We generated a *Ddx3x* haploinsufficient mouse (*Ddx3x*$^{+/-}$ females) with construct validity for *DDX3X* loss-of-function mutations. We used standardized batteries to assess developmental milestones and adult behaviors, as well as magnetic resonance imaging and immunostaining of cortical projection neurons to capture early postnatal changes in brain development.

Results: *Ddx3x*$^{+/-}$ females show physical, sensory, and motor delays that evolve into behavioral anomalies in adulthood, including hyperactivity, anxiety-like behaviors, cognitive impairments in specific tasks (e.g., contextual fear memory but not novel object recognition memory) and motor deficits. Motor function declines with age but not if mice were previously exposed to behavioral training. Developmental and behavioral changes are associated with a reduction in brain volume, with some regions (e.g., cortex and amygdala) disproportionally affected. Cortical thinning is accompanied by defective cortical lamination, indicating that *Ddx3x* regulates the balance of glutamatergic neurons in the developing cortex.

Conclusions: These data shed new light on the developmental mechanisms driving DDX3X syndrome and support face validity of this novel pre-clinical mouse model.

Keywords

DDX3X syndrome; intellectual disability; movement disorder; corticogenesis; neurodevelopment

INTRODUCTION

DDX3X syndrome accounts for ~2% of intellectual disability/developmental delay (ID/DD) in females (1, 2). The syndrome presents with a constellation of co-morbidities, including low body weight, hypotonia and/or hypertonia with spasticity, microcephaly, seizures, movement disorders, behavioral problems, and brain malformations (1, 3, 4).

DDX3X syndrome is due to mutations in the DExD/H-box RNA helicase DDX3X (1, 2), which facilitates the ATP-dependent unwinding of RNA secondary structures and affects RNA metabolism, especially mRNA translation (3, 5-7). *DDX3X* is on the X chromosome but it escapes X chromosome inactivation (8, 9). As a result, females express two alleles, while males can only express one. The *DDX3X* paralog on the Y chromosome (*DDX3Y*) does not appear to compensate for this dosage imbalance as it is translated only in spermatocytes (10). Consistently, *DDX3Y* deletions cause subfertility/infertility (11).

Females with DDX3X syndrome carry *de novo* loss-of-function mutations plausibly leading to haploinsufficiency or missense/in-frame mutations (1-3). Some missense/in-frame mutations are associated with more severe phenotypes (3). Only a few affected males—all carrying missense mutations—have been identified (1, 3, 12, 13). These males often inherit the mutations from their mothers, who appear asymptomatic. This observation, alongside functional data in zebrafish (1, 13), suggests that the male mutations act as hypomorphic alleles.

The mechanisms underlying DDX3X syndrome are beginning to emerge. *Ddx3x* is required for mouse embryogenesis (14), hindbrain development (15), corticogenesis (3), and synaptogenesis (7). *Ddx3x* germline knockout disrupts placentation and lead to lethality at embryonic day (E) 6.5 (14). Restricting the knockout to embryonic tissues nevertheless alters embryogenesis: *Ddx3x* null male embryos show multiple anomalies and die at ~E11.5 (14). *Ddx3x* haploinsufficient females have not been thoroughly characterized (14). Mice with brain-specific *Ddx3x* knockout (in neural stem cells starting at E9.5) survive but show altered brain growth, accompanied by ataxia and seizures (15). Prenatal knockdown of ~25% *Ddx3x* in cortical neuronal progenitors at E14.5 impacts their differentiation into neurons (3). Postnatal *Ddx3x* knockdown disrupts neurite outgrowth, and dendritic spine formation and maturation (7). How these cellular functions relate to behavior is unknown.

We present a novel *Ddx3x* haploinsufficient mouse ($Ddx3x^{+/-}$ females) with construct validity for *DDX3X* loss-of-function mutations found in females. We show evidence for awry developmental trajectories that precede adult behavioral abnormalities. These phenotypes are accompanied by reduced brain volume consequent to the overall growth delay and alterations in the cytoarchitecture of the developing cortex.

METHODS AND MATERIALS

Mice.

Animal procedures were approved by the Institutional Animal Care and Use Committee of the Icahn School of Medicine at Mount Sinai. The $Ddx3x^{flox}$ line was generated at Ozgene by introducing two loxP sites flanking exon 2 of mouse *Ddx3x* (OTTMUSG00000017078) in C57BL/6J embryonic stem cells. To generate the knockout allele, $Ddx3x^{flox/flox}$ females were crossed with B6.Cg-Edil3$^{Tg(Sox2-Cre)1Amc}$/J males (Sox2-Cre/+) (16) (The Jackson Laboratory, #008454). The colony was maintained on a C57BL/6J background. Additional information is in Supplemental Note.

Developmental milestones.

Testing was performed as in (17). Four cohorts were tested (Table S1; Cohort 1: 17 $Ddx3x^{+/+}$; 7 $Ddx3x^{+/-}$; 16 $Ddx3x^{+/y}$; Cohort 2: 7 $Ddx3x^{+/+}$; 6 $Ddx3x^{+/-}$; 7 $Ddx3x^{+/y}$; Cohort 3: 5 $Ddx3x^{+/+}$; 3 $Ddx3x^{+/-}$; 8 $Ddx3x^{+/y}$; Cohort 4: 19 $Ddx3x^{+/+}$; 13 $Ddx3x^{+/-}$; 13 $Ddx3x^{+/y}$). Given the low numbers in Cohort 3, data in this cohort are considered as preliminary corroborations. As additional control, we tested a cohort of Sox2-Cre/+ mice (Table S3). To control for litter size effects, litters were limited to 6 pups per dam by adding excess pups to smaller litters on P1. Each test is described in Supplemental Note.

Behavioral testing.

Four cohorts of adult (4-month old) mice and two cohorts of ageing (one-year old) mice were tested (Table S2; Adults: Cohort 1: 9 $Ddx3x^{+/+}$; 5 $Ddx3x^{+/-}$; Cohort 2: 16 $Ddx3x^{+/+}$; 23 $Ddx3x^{+/-}$; Cohort 3: 16 $Ddx3x^{+/+}$; 16 $Ddx3x^{+/-}$; Cohort 4: 12 $Ddx3x^{+/+}$; 12 $Ddx3x^{+/-}$; Ageing: Cohort 1: 13 $Ddx3x^{+/+}$; 6 $Ddx3x^{+/-}$; Cohort 2: 10 $Ddx3x^{+/+}$; 11 $Ddx3x^{+/-}$). Given the low numbers in adult Cohort 1, data in this cohort are considered as preliminary corroborations. Adult cohort 3 was followed up at one year of age (“pre 1yr” ,Table

S2). Testing was conducted during the light phase in sound-attenuated rooms. Mice were habituated to the testing room for 30 min prior to testing. The two genotypes were tested on the same day in randomized order by an experimenter blind to genotype. Handling and specific tests are described in Supplemental Note.

Magnetic resonance imaging.

Procedures are described in Supplemental Note.

Immunostaining.

Brains were fixed in 4% PFA in PBS overnight at 4°C, and then cryopreserved in 30% (w/v) sucrose, 0.05% sodium azide and 100mM glycine in PBS. Brains were embedded in Tissue-Tek® O.C.T. Compound (VWR) and sectioned using a Leica CM1860 cryostat (40μm). Sections were washed in PBS + 0.05% Triton X-100 (Thermo Scientific) and blocked with 5% donkey serum (Sigma) for 1 hr at room temperature. Sections from adult brains underwent antigen retrieval (Supplemental Note). Primary antibodies were incubated overnight at 4°C in the dark. After washing in PBS + 0.05% Triton X-100, sections were incubated for 2 hrs at room temperature with secondary antibodies. Antibody information and imaging procedures are in Supplemental Note.

Statistical analyses.

Data were scored and analyzed blind to genotype. Statistics and plots were generated using custom R scripts. Outliers were identified as data points below Q1-1.5xIQR or above Q3+1.5xIQR (Q1, first quartile; Q3, third quartile; IQR, interquartile range) and removed. Repeated measure ANOVA was used for repeated observations. For comparisons between two groups, Shapiro–Wilk test was used to assess normality, followed by Student's t-test for normally distributed data (equal variance), Welch's t-test for normally distributed data (unequal variance), or Wilcoxon signed-rank test for not normally distributed data. For multiple comparisons, two-way ANOVA test was employed.

RESULTS

A novel mouse with construct validity for DDX3X syndrome.

We generated a novel mouse with construct validity for loss-of-function mutations clinically associated with DDX3X syndrome. We first generated a floxed line (*Ddx3x*^{flox}) by introducing loxP sites flanking exon 2. We selected this exon because it has 100% identity with the human sequence and there are at least 13 individuals with pathogenic loss-of-function mutations affecting this exon (Fig. S1A). As *Ddx3x* is indispensable for placentation in mouse (14), we adopted the strategy used by Chen et al (2015) (14) and used a Sox2-Cre driver line to induce recombination only in the epiblast at early gastrulation (16). The resulting progeny develop with a functional placenta (14).

We crossed *Ddx3x*$^{flox/flox}$ females with Sox2-Cre/+ males to excise exon 2 and generate a *Ddx3x* targeted allele (Fig. S1B-C). This breeding scheme is expected to generate: *Ddx3x*$^{flox/+}$;+/+ females (hereafter referred to as *Ddx3x*$^{+/+}$), *Ddx3x*$^{flox/y}$;+/+ males (*Ddx3x*$^{+/y}$), *Ddx3x*$^{flox/+}$;Sox2-Cre/+ females (*Ddx3x*$^{+/-}$), and, *Ddx3x*$^{flox/y}$;Sox2-Cre/+

males (*Ddx3x*$^{-/y}$). In line with earlier findings (14) and the dearth of male patients with pathogenic mutations in *DDX3X*, *Ddx3x*$^{-/y}$ male embryos died *in utero* (Fig. S1D). *Ddx3x*$^{+/-}$ females survived to adulthood (27/32 *Ddx3x*$^{+/+}$ vs. 22/23 *Ddx3x*$^{+/-}$ females reached 18 months of life, Fisher's exact test, p=0.3). At a histopathological examination, P3 *Ddx3x*$^{+/-}$ pups showed no gross anatomical differences (n=5/genotype). 4/5 *Ddx3x*$^{+/-}$ and 1/5 *Ddx3x*$^{+/+}$ pups had acute suppurative alveolitis consistent with aspiration pneumonitis (Fisher's exact test, p=0.2).

We next measured *Ddx3x* expression in the cortex of the three genotypes. Female control mice had higher *Ddx3x* mRNA and protein than males (Fig. S1E-G), as expected given that *DDX3X* is an escape gene (8, 9). *Ddx3x*$^{+/-}$ females had ~40% reduction in *Ddx3x* mRNA and protein compared to control females (Fig. S1E-G), confirming that *Ddx3x*$^{+/-}$ mice recapitulate haploinsufficiency. Expression of key synaptic proteins in P21 mice appeared unaffected (Fig. S1H-I).

Ddx3x$^{+/-}$ females have developmental delays.

We monitored *Ddx3x*$^{+/-}$ mice from birth to weaning using a standardized observation battery (18) adapted from the Fox scale (19, 20). Data were collected blind to genotype and across four independent cohorts (Table S1). As control, we also tested a cohort of Sox2-Cre/+ male and female pups (and littermate controls) and confirmed the lack of effects driven by Sox2-Cre allele (Table S3).

Ddx3x$^{+/-}$ pups had a growth delay (Fig. 1A) manifesting as lower body weight in adulthood (Fig. 1A-B). Growth positively correlated with litter size for all genotypes (Fig. S2), suggesting that *Ddx3x*$^{+/-}$ pups were not outcompeted by their siblings for access to maternal milk supply. The rate of aspiration pneumonitis, combined with the failure to thrive, suggests that *Ddx3x*$^{+/-}$ pups had reduced competence in feeding. These observations align with the low body weight and feeding problems in patients (1, 3, 4). Further, *Ddx3x*$^{+/-}$ pups had a delay in eye opening (Fig. 1C) and pinna detachment (Fig. S3A). No delays were noted in the development of the fur/skin or tooth eruption (Fig. S3B-D).

Physical delays were accompanied by delays in processing sensory cues. Delayed eye opening (Fig. 1C) translated into a delay in establishing visual placing competence (Fig. 1D). *Ddx3x*$^{+/-}$ pups were delayed in developing a startle reflex to an auditory stimulus (Fig. 1E) and a labyrinth-related reflex measured as aversion to a cliff edge (Fig. S3E). Both alterations could be related to delayed ear development (Fig. S3A). Responses to tactile cues varied: *Ddx3x*$^{+/-}$ pups had delays in ear twitch reflex (Fig. 1F) and vibrissae-evoked forelimb placing (Fig. S3F), but not in forelimb grasping reflex (Fig. S3G).

Ddx3x$^{+/-}$ pups had motor delays. *Ddx3x*$^{+/-}$ pups took longer to flip onto their paws from a supine position (righting reflex) (Fig. 2A), indicative of hypotonia. Motor coordination in response to vestibular cues of gravity was also affected, as measured by delayed acquisition of negative geotaxis skills (Fig. 2B-C). Neuromuscular development was abnormal, as *Ddx3x*$^{+/-}$ pups showed alterations in forelimbs and hindlimbs grip (Fig. 2D-E, Fig. S4A). No defects in locomotor activity in open field (Fig. S4B) or air righting reflex (Fig. S4C) were noted.

Overall, *Ddx3x*$^{+/-}$ female pups follow abnormal trajectories of physical, sensory, and motor development.

Ddx3x$^{+/-}$ females have hyperactivity, anxiety-related behaviors, and associative memory deficits.

The sensorimotor delays might alter the timing of critical periods for brain development and plasticity and translate into behavioral abnormalities later in life. We therefore examined emotion states, cognition, and sociability of *Ddx3x*$^{+/-}$ adult mice using a behavioral testing battery. Data were collected blind to genotype, and across four independent cohorts not employed for developmental testing (Table S2). During handling one week prior to testing, we noted no differences in physical appearance other than lower body weight (Fig. 1B). *Ddx3x*$^{+/-}$ mice, however, showed changes in spontaneous general activity (Fig. S5A), reduced limb withdrawal indicative of reduced nociception (Fig. S5B), and reduced provoked biting reflex (Fig. S5C). We also noted a higher defecation index (Fig. S5D).

When assessed for free locomotor activity in an open field test, *Ddx3x*$^{+/-}$ mice explored the arena more and moved faster than controls (Fig. 3A-B, Fig. S6A). These observations indicate hyperactivity. While *Ddx3x*$^{+/-}$ mice entered the center zone as often as controls (Fig. S6B), it took them longer to enter it and they spent less time in it (Fig. 3C-D). This increase in latency and degree of thigmotaxis indicate an anxiety-like behavior. *Ddx3x*$^{+/-}$ mice did not show, however, gross deficits in an elevated plus maze test (Fig. S6C).

We measured short-term working memory using a Y maze spontaneous alternation test. *Ddx3x*$^{+/-}$ mice explored the arms more than controls (Fig. 3E), corroborating the hyperactivity observed in open field. There was no difference in the number of spontaneous alternations (‘ABC’, Fig. 3F), but *Ddx3x*$^{+/-}$ mice re-entered the same arm after exploring a new one at higher frequency (error ‘ABA’). Overall, these data suggest no overt deficits in short-term working memory.

Next, we tested associative learning and memory using the contextual and cued fear conditioning paradigm. After habituation and prior to training, both genotypes showed low baseline levels of freezing response (Fig. 3G). During training, mice were exposed to three tone-shock pairs. After 24 hours, mice were placed in the same context without presentation of tone or shock. While both genotypes showed a freezing behavior elicited by the context, which increased over time, initial recall was weaker in *Ddx3x*$^{+/-}$ mice (Fig. 3H). The deficit was specific to contextual memory, as *Ddx3x*$^{+/-}$ mice showed the intact freezing behavior evoked by the tone in a new context (Fig. 3I). Since *Ddx3x*$^{+/-}$ mice were indistinguishable from controls during training or cued testing (Fig. 3G, 3I), reduced freezing in contextual testing is not a manifestation of hyperactivity but a genuine memory deficit. *Ddx3x*$^{+/-}$ mice did not show differences in recognition memory in a novel object recognition task (Fig. 3J) or sociability measured in a three-chamber social approach test (Fig. S7).

Together, these data show that *Ddx3x*$^{+/-}$ mice display hyperactivity and anxiety-like behaviors, accompanied by contextual fear memory deficits.

Ddx3x$^{+/-}$ females have motor deficits.

Movement disorders and gait abnormalities are prevalent in the patient population (1, 3, 4) and *Ddx3x*$^{+/-}$ pups display motor delays (Fig. 2). To examine motor function later in life, we first assessed gait. We found a transient alteration in gait, with changes at P19 and P22 that were no longer apparent by P30 (Fig. S8). Next we used the accelerating rotarod test to measure motor coordination, endurance, and learning over two days, 24 hrs apart, each including 3 trials. Adult (4-month old) mice of both genotypes improved their performance (latency to fall) over the trials, showing no deficits in short-term or long-term learning (Fig. 4A). However, the motor performance of *Ddx3x*$^{+/-}$ mice was suboptimal, as they had a shorter latency to fall (Fig. 4A).

While the natural history of DDX3X syndrome has yet to be mapped, the oldest affected female reported so far (47 year old) had motor decline (4). We therefore probed motor function in one-year old mice. In the rotarod paradigm employed at 4 months, one-year mice showed reduced endurance, irrespective of genotype. *Ddx3x*$^{+/-}$ mice did not show deficits (Fig. S9). To dissect learning in greater depth, we conducted rotarod testing over 3 days, 24 hrs apart, each including 4 trials, in two independent cohorts of one-year old mice (Table S2). In addition to poor motor performance, one-year old *Ddx3x*$^{+/-}$ mice showed a decline in motor function and learning (Fig. 3B).

To further assess fine motor coordination and balance, we used a balance beam test and a vertical pole test. 4-month old *Ddx3x*$^{+/-}$ mice covered a shorter distance on the balance beam and slipped more frequently than controls (Fig. 4C-D). One-year old *Ddx3x*$^{+/-}$ mice had a more pronounced loss of balance (Fig. 4C-D). To understand the impact of prior behavioral training, a 4-month old cohort was re-tested at one year of age (Table S2) (“pre 1yr” group). This group showed no impairments in the balance beam test (Fig. 4C-D). When climbing on a vertical pole, 4-month old *Ddx3x*$^{+/-}$ mice had no deficits in turning but it took them longer to descend the pole (Fig. 4E-F). Naïve one-year old *Ddx3x*$^{+/-}$ mice had difficulties both turning and descending, but not the pre-exposed one-year old group (Fig. 4E-F).

As for neuromuscular strength, although 4 month-old mice *Ddx3x*$^{+/-}$ mice were able to hang on a wire as long as their littermates, they covered a reduced number of segments while moving on the wire (Fig. 4G-H), indicating intact motor endurance but altered coordination. Ageing animals of both genotypes had, as expected, reduced strength. Naïve, but not pre-exposed *Ddx3x*$^{+/-}$ mice, performed worse than controls (Fig. 4G).

Overall, *Ddx3x* haploinsufficiency causes motor deficits exacerbated with ageing, but prior exposure to behavioral training can alleviate motor decline.

Ddx3x$^{+/-}$ females have reduced brain volume, with some regions disproportionally affected.

Individuals with DDX3X syndrome frequently have microcephaly and brain malformations (1, 3, 4). Therefore, we performed magnetic resonance imaging (MRI) on pups at P3, a stage where developmental delays begin to emerge. *Ddx3x*$^{+/-}$ pups had a ~10% reduction in overall brain volume (n=10/genotype; Student’s t test, p=0.03) (Fig. 5, Fig. S10, Table S4).

These brain volumes differences were no longer apparent when normalized to body weight (Table S4), indicating that these changes are part of an overall growth delay, not a pure microcephaly phenotype.

To identify brain regions with a larger deviation, we focused on those that were either larger (<8%) or smaller (>12%) reduction than expected (based on the ~10% overall reduction). We found volumetric reduction disproportionally in the neocortex, part of the olfactory system (olfactory bulbs, the olfactory tubercle, and the lateral olfactory tract), and part of the limbic system (amygdala and the hippocampus, especially the subiculum) (Fig. 5C, Table S4).

Overall, *Ddx3x* haploinsufficiency causes a growth delay that affects brain development, with changes in specific brain regions functionally relating with behavioral deficits.

Ddx3x$^{+/-}$ females have abnormal neocortical lamination.

Given that the cortex is disproportionally smaller in *Ddx3x*$^{+/-}$ pups (Fig. 3) and cortical malformations are common in DDX3X syndrome (1, 3, 4), we examined the main glutamatergic projection neurons in the developing cortex. Intra-telencephalic neurons (IT) residing in both upper layers (UL) and deep layers (DL) project to the ipsilateral or contralateral cortex, the latter through the corpus callosum (callosal projection neurons, CPN). Corticofugal neurons residing in DL project to subcerebral targets (ScPN mostly in layer V) or thalamus (CthPN mostly in layer VI). ScPN are marked by CTIP2/BCL11B (21-28), while CthPN express TBR1 (29, 30). UL IT express BRN1/POU3F3 (31-33), while UL or DL CPN express SATB2 (21-25), with the caveat that SATB2 is detected also in a minority of CTIP2+ ScPN (26, 27). Using these population-specific markers, we immunostained brain sections from P3 pups. We first examined the total number of cells (DAPI+), CTIP2+, BRN1+ or SATB2+ neurons in coronal sections from primary (M1) and secondary (M2) motor cortices. We observed a higher number of cells in M2 of *Ddx3x*$^{+/-}$ mice (Fig. S11). This increase was largely attributable to an excess of CTIP2+ neurons, which showed a ~1.5 fold increase in *Ddx3x*$^{+/-}$ cortices compared to controls (Fig. S11). There was also a modest excess of CTIP2+ neurons in M1, which did not, however, lead to a significant increase in the total number of cells (Fig. S11).

We then examined the relative distribution of CTIP2+, BRN1+, or SATB2+ populations across ten equally sized bins from the pia to the ventricle of M1. The distribution of CTIP2+ neurons was altered in M1 of *Ddx3x*$^{+/-}$ mice: most CTIP2+ neurons were, as expected, in layer V, but a fraction extended deeper (Fig. 6A-B). These differences were not noted in M2 (Fig. S12). In *Ddx3x*$^{+/-}$ mice, UL and DL SATB2+ CPN were unaffected (S13A-C), while the TBR1+ CthPN pool was increased in DL (Fig. S13D-F).

CTIP2 and BRN1 are mostly mutually exclusive, but a subpopulation of neurons expressing both markers appears in the presumptive layer V at E15.5 and is still visible at P0 (31). We therefore asked whether the misplaced CTIP2+ neurons in *Ddx3x*$^{+/-}$ mice could be BRN1+. We counted the CTIP2+BRN1+ cells in bins 5-7 of M1, and found that they were excessive in *Ddx3x*$^{+/-}$ mice (Fig. 6D-E). Given this surplus, we monitored the CTIP2+SATB2+ subpopulation, which emerges after birth and includes ScPN and CPN (26), and a

corticospinal CTIP2+SATB2+ subpopulation co-expressing BHLHB5 (26) restricted to the caudal motor and sensory cortex by P0 (34). We found fewer DL CTIP2+SATB2+ cells in M1 of *Ddx3x*$^{+/-}$ mice, but no specific changes in corticospinal CTIP2+SATB2+BHLHB5+ (Fig. S14). Overall, in the motor cortex, the cortices of *Ddx3x*$^{+/-}$ pups show alteration of location and specification of CTIP2+ subpopulations (both ScPN and ITs), with excess of CTIP2+BRN1+ and depletion of CTIP2+SATB2+ subpopulations.

Given the sensory delays observed in *Ddx3x*$^{+/-}$ pups (e.g., Fig. 1F), we extended our analyses to the primary somatosensory cortex (S1). We observed alterations distinct from those seen in the motor cortex. *Ddx3x*$^{+/-}$ S1 displayed fewer CTIP2+ neurons (Fig. S11A, E), especially in layer V (Fig. 6F, G), and more BRN1+ neurons (Fig. S11E), but no changes in CTIP2+BRN1+ (Fig. 6I-J) or CTIP2+SATB2+ subpopulations (Fig. S14A-C). Hence, in S1 there are defects in the abundance of CTIP2+ ScPN and BRN1+ IT neurons, without altered specification of subpopulations.

Finally, given that most anomalies relate to CTIP2+ neurons, we followed their distribution in the M1, M2, and S1 of adult (4-month old) mice. Irrespective of cortical area, DL CTIP2+ neurons were reduced in *Ddx3x*$^{+/-}$ mice (Fig. S15), indicating that cortical alterations are maintained throughout adulthood.

In conclusion, *Ddx3x* haploinsufficiency causes defects in the balance of glutamatergic projection neurons in the developing and adult cortex.

DISCUSSION

Altered somatosensation is emerging as a critical symptom in neurodevelopmental disorders (35) and is captured in the phenotype of several mouse models (17, 36-41). *Ddx3x*$^{+/-}$ pups are delayed in responding to visual, auditory, and tactile cues. Further, *Ddx3x*$^{+/-}$ pups have an underdeveloped olfactory system, which might suggest impaired olfaction. Abnormal sensory experience during early postnatal life robustly affects cortical plasticity and adult behavior, as shown by sensory deprivation in mice (42-45). The delay in eye opening in *Ddx3x*$^{+/-}$ pups might delay cortical maturation, given that dark rearing shifts the onset of the critical period (46-48). Further, *Ddx3x*$^{+/-}$ pups have defects in the development of the somatosensory cortex already detectable at P3, prior to the peak of critical period plasticity in the second postnatal week (48). Hence, the adult manifestations in *Ddx3x*$^{+/-}$ mice might be rooted in congenital cortical defects and possibly a further delay in cortical maturation due to disrupted sensory stimuli exposure.

Motor dysfunction is one of earliest signs raising clinical concerns and a prominent trait in DDX3X syndrome (1, 3, 4). Motor development follows a complex trajectory in *Ddx3x*$^{+/-}$ mice. Early anomalies (postnatal hypotonia and abnormal gait in juvenile age) evolve into changes in coordination in adulthood and further loss of balance and endurance with ageing. Cortical circuits subserving these functions include the corticopontine and corticospinal tracts formed by the ScPN. As ScPN are altered in the motor cortex of *Ddx3x*$^{+/-}$ mice, defective corticopontine and/or corticospinal circuits might contribute to the motor phenotype. Small pons and small inferior vermis can be observed in individuals

with DDX3X syndrome (3), suggesting that the cortico-ponto-cerebellar tract might be altered. Divergence in motor circuits between species might explain the transient nature of certain motor deficits in mice. For example, the rubrospinal tract, which can compensate for corticospinal lesions even in adulthood (49), is underdeveloped in humans compared to mice.

Ddx3x$^{+/-}$ mice show anxiety-like behaviors, hyperactivity, and weaker initial context-dependent recall of fear memory, but no changes in cue-elicited fear memory or novel object recognition. Albeit complex and interlinked, the circuits subserving these behaviors require the cortex, the amygdala, and the hippocampus (50-52), all found disproportionally diminished in volume in *Ddx3x*$^{+/-}$ mice. Additionally, mouse models of neurodevelopmental disorders often show similar behavioral anomalies contingent to altered balance of cortical glutamatergic populations (30, 53, 54). *Ddx3x*$^{+/-}$ mice show an area-specific altered balance of cortical glutamatergic populations that might result from changes neurogenesis, migration and/or cell fate specification. These findings and those by Lennox et al (2020) (3) on DDX3X add on the growing body of evidence showing the importance of mRNA translation for cortical development (55-60).

Our model has validity for loss-of-function mutations leading to haploinsufficiency. Clinical and functional data (3) suggest that there is at least a second disease mechanism at play, with certain missense mutations acting as gain-of-function and leading to more severe clinical outcomes, e.g. polymicrogyria (3). Our model is less informative with respect to this group of mutations. One hint to this limitation relates to hypotonia. While individuals with missense mutations associated with polymicrogyria often exhibit a mix of hypertonia and hypotonia, those with loss-of-function mutations are disproportionally affected by hypotonia (3), as do *Ddx3x*$^{+/-}$ mice. However, most missense mutations do not yield polymicrogyria and likely act as hypomorphic alleles. We expect these mutations to yield a phenotype similar, but attenuated, to that of *Ddx3x*$^{+/-}$ mice. Modeling missense mutations in mice will help discriminate the various mechanisms driving DDX3X syndrome.

Our data suggest that motor function in *Ddx3x*$^{+/-}$ mice can change with time and is sensitive to prior exposure to behavioral training. Therefore, the DDX3X pathology is engrained in prenatal development but also maintained in adulthood. These findings motivate longitudinal studies in the patient population and might help identify the temporal windows where pathology (and thus phenotype) can be modified. These two lines of work, alongside a better understanding of the disease mechanisms at play, are important next steps for designing therapies for DDX3X syndrome.

Supplementary Material

Refer to Web version on PubMed Central for supplementary material.

ACKNOWLEDGMENTS AND DISCLOSURES

Research reported in this publication was supported by the Eunice Kennedy Shriver National Institute Of Child Health & Human Development of the National Institutes of Health under Award Numbers R01HD104609 and R21HD097561 (to SDR). The content is solely the responsibility of the authors and does not necessarily represent the official views of the National Institutes of Health. The work was also supported by the Beatrice and Samuel A.

Seaver Foundation, the Friedman Brain Institute Research Award by the Fascitelli Family, and the Distinguished Scholar Award from the Icahn School of Medicine at Mount Sinai. DCU was supported by Fondation pour la Recherche Médicale, the Philippe Foundation, and the Beatrice and Samuel A. Seaver Foundation. MGF was supported by the Beatrice and Samuel A. Seaver Foundation and the Fundación Alfonso Martín Escudero. MF was supported by a Dean's Undergraduate Research Fund Grant for Spring and Fall 2020. We thank Dr. Ki Goosens for providing expertise on behavioral testing. We thank Brett Collins for lab managing support and Zeynep Akpinar for technical support. LRQ, JE, and JPL would like to acknowledge support from the Ontario Brain Institute and the Canadian Institute for Health Research. The preprint version of the manuscript was deposited in BioRxiv (#2021.01.22.427482).

REFERENCES

1. Snijders Blok L, Madsen E, Juusola J, Gilissen C, Baralle D, Reijnders MR, et al. (2015): Mutations in DDX3X Are a Common Cause of Unexplained Intellectual Disability with Gender-Specific Effects on Wnt Signaling. American journal of human genetics. 97:343–352. [PubMed: 26235985]
2. DDD Study (2017): Prevalence and architecture of de novo mutations in developmental disorders. Nature. 542:433–438. [PubMed: 28135719]
3. Lennox AL, Hoye ML, Jiang R, Johnson-Kerner BL, Suit LA, Venkataramanan S, et al. (2020): Pathogenic DDX3X Mutations Impair RNA Metabolism and Neurogenesis during Fetal Cortical Development. Neuron. 106:404–420 e408. [PubMed: 32135084]
4. Wang X, Posey JE, Rosenfeld JA, Bacino CA, Scaglia F, Immken L, et al. (2018): Phenotypic expansion in DDX3X - a common cause of intellectual disability in females. Ann Clin Transl Neurol. 5:1277–1285. [PubMed: 30349862]
5. Valentin-Vega YA, Wang YD, Parker M, Patmore DM, Kanagaraj A, Moore J, et al. (2016): Cancer-associated DDX3X mutations drive stress granule assembly and impair global translation. Sci Rep. 6:25996. [PubMed: 27180681]
6. Soto-Rifo R, Rubilar PS, Limousin T, de Breyne S, Decimo D, Ohlmann T (2012): DEAD-box protein DDX3 associates with eIF4F to promote translation of selected mRNAs. EMBO J. 31:3745–3756. [PubMed: 22872150]
7. Chen HH, Yu HI, Tarn WY (2016): DDX3 Modulates Neurite Development via Translationally Activating an RNA Regulon Involved in Rac1 Activation. J Neurosci. 36:9792–9804. [PubMed: 27656019]
8. Garieri M, Stamoulis G, Blanc X, Falconnet E, Ribaux P, Borel C, et al. (2018): Extensive cellular heterogeneity of X inactivation revealed by single-cell allele-specific expression in human fibroblasts. Proc Natl Acad Sci U S A. 115:13015–13020. [PubMed: 30510006]
9. Tukiainen T, Villani AC, Yen A, Rivas MA, Marshall JL, Satija R, et al. (2017): Landscape of X chromosome inactivation across human tissues. Nature. 550:244–248. [PubMed: 29022598]
10. Ditton HJ, Zimmer J, Kamp C, Rajpert-De Meyts E, Vogt PH (2004): The AZFa gene DBY (DDX3Y) is widely transcribed but the protein is limited to the male germ cells by translation control. Hum Mol Genet. 13:2333–2341. [PubMed: 15294876]
11. Foresta C, Ferlin A, Moro E (2000): Deletion and expression analysis of AZFa genes on the human Y chromosome revealed a major role for DBY in male infertility. Hum Mol Genet. 9:1161–1169. [PubMed: 10767340]
12. Nicola P, Blackburn PR, Rasmussen KJ, Bertsch NL, Klee EW, Hasadsri L, et al. (2019): De novo DDX3X missense variants in males appear viable and contribute to syndromic intellectual disability. American journal of medical genetics Part A. 179:570–578. [PubMed: 30734472]
13. Kellaris G, Khan K, Baig SM, Tsai IC, Zamora FM, Ruggieri P, et al. (2018): A hypomorphic inherited pathogenic variant in DDX3X causes male intellectual disability with additional neurodevelopmental and neurodegenerative features. Hum Genomics. 12:11. [PubMed: 29490693]
14. Chen CY, Chan CH, Chen CM, Tsai YS, Tsai TY, Wu Lee YH, et al. (2016): Targeted inactivation of murine Ddx3x: essential roles of Ddx3x in placentation and embryogenesis. Hum Mol Genet. 25:2905–2922. [PubMed: 27179789]
15. Patmore DM, Jassim A, Nathan E, Gilbertson RJ, Tahan D, Hoffmann N, et al. (2020): DDX3X Suppresses the Susceptibility of Hindbrain Lineages to Medulloblastoma. Dev Cell.

16. Hayashi S, Lewis P, Pevny L, McMahon AP (2002): Efficient gene modulation in mouse epiblast using a Sox2Cre transgenic mouse strain. Mech Dev. 119 Suppl 1:S97–S101. [PubMed: 14516668]
17. Drapeau E, Riad M, Kajiwara Y, Buxbaum JD (2018): Behavioral Phenotyping of an Improved Mouse Model of Phelan-McDermid Syndrome with a Complete Deletion of the Shank3 Gene. eNeuro. 5.
18. Drapeau E, Dorr NP, Elder GA, Buxbaum JD (2014): Absence of strong strain effects in behavioral analyses of Shank3-deficient mice. Disease models & mechanisms. 7:667–681. [PubMed: 24652766]
19. Fox WM (1965): Reflex-ontogeny and behavioural development of the mouse. Anim Behav. 13:234–241. [PubMed: 5835840]
20. Heyser CJ (2004): Assessment of developmental milestones in rodents. Curr Protoc Neurosci. Chapter 8:Unit 8 18.
21. Alcamo EA, Chirivella L, Dautzenberg M, Dobreva G, Farinas I, Grosschedl R, et al. (2008): Satb2 regulates callosal projection neuron identity in the developing cerebral cortex. Neuron. 57:364–377. [PubMed: 18255030]
22. Arlotta P, Molyneaux BJ, Chen J, Inoue J, Kominami R, Macklis JD (2005): Neuronal subtype-specific genes that control corticospinal motor neuron development in vivo. Neuron. 45:207–221. [PubMed: 15664173]
23. Baranek C, Dittrich M, Parthasarathy S, Bonnon CG, Britanova O, Lanshakov D, et al. (2012): Protooncogene Ski cooperates with the chromatin-remodeling factor Satb2 in specifying callosal neurons. Proc Natl Acad Sci U S A. 109:3546–3551. [PubMed: 22334647]
24. Britanova O, de Juan Romero C, Cheung A, Kwan KY, Schwark M, Gyorgy A, et al. (2008): Satb2 is a postmitotic determinant for upper-layer neuron specification in the neocortex. Neuron. 57:378–392. [PubMed: 18255031]
25. Srivatsa S, Parthasarathy S, Britanova O, Bormuth I, Donahoo AL, Ackerman SL, et al. (2014): Unc5C and DCC act downstream of Ctip2 and Satb2 and contribute to corpus callosum formation. Nat Commun. 5:3708. [PubMed: 24739528]
26. Harb K, Magrinelli E, Nicolas CS, Lukianets N, Frangeul L, Pietri M, et al. (2016): Area-specific development of distinct projection neuron subclasses is regulated by postnatal epigenetic modifications. Elife. 5:e09531. [PubMed: 26814051]
27. Leone DP, Heavner WE, Ferenczi EA, Dobreva G, Huguenard JR, Grosschedl R, et al. (2015): Satb2 Regulates the Differentiation of Both Callosal and Subcerebral Projection Neurons in the Developing Cerebral Cortex. Cereb Cortex. 25:3406–3419. [PubMed: 25037921]
28. Canovas J, Berndt FA, Sepulveda H, Aguilar R, Veloso FA, Montecino M, et al. (2015): The Specification of Cortical Subcerebral Projection Neurons Depends on the Direct Repression of TBR1 by CTIP1/BCL11a. J Neurosci. 35:7552–7564. [PubMed: 25972180]
29. McKenna WL, Betancourt J, Larkin KA, Abrams B, Guo C, Rubenstein JL, et al. (2011): Tbr1 and Fezf2 regulate alternate corticofugal neuronal identities during neocortical development. J Neurosci. 31:549–564. [PubMed: 21228164]
30. Fazel Darbandi S, Robinson Schwartz SE, Qi Q, Catta-Preta R, Pai EL, Mandell JD, et al. (2018): Neonatal Tbr1 Dosage Controls Cortical Layer 6 Connectivity. Neuron. 100:831–845 e837. [PubMed: 30318412]
31. Dominguez MH, Ayoub AE, Rakic P (2013): POU-III transcription factors (Brn1, Brn2, and Oct6) influence neurogenesis, molecular identity, and migratory destination of upper-layer cells of the cerebral cortex. Cereb Cortex. 23:2632–2643. [PubMed: 22892427]
32. Sugitani Y, Nakai S, Minowa O, Nishi M, Jishage K, Kawano H, et al. (2002): Brn-1 and Brn-2 share crucial roles in the production and positioning of mouse neocortical neurons. Genes Dev. 16:1760–1765. [PubMed: 12130536]
33. Oishi K, Aramaki M, Nakajima K (2016): Mutually repressive interaction between Brn1/2 and Rorb contributes to the establishment of neocortical layer 2/3 and layer 4. Proc Natl Acad Sci U S A. 113:3371–3376. [PubMed: 26951672]

34. Joshi PS, Molyneaux BJ, Feng L, Xie X, Macklis JD, Gan L (2008): Bhlhb5 regulates the postmitotic acquisition of area identities in layers II-V of the developing neocortex. Neuron. 60:258–272. [PubMed: 18957218]
35. Green SA, Hernandez L, Tottenham N, Krasileva K, Bookheimer SY, Dapretto M (2015): Neurobiology of Sensory Overresponsivity in Youth With Autism Spectrum Disorders. JAMA Psychiatry. 72:778–786. [PubMed: 26061819]
36. He CX, Cantu DA, Mantri SS, Zeiger WA, Goel A, Portera-Cailliau C (2017): Tactile Defensiveness and Impaired Adaptation of Neuronal Activity in the Fmr1 Knock-Out Mouse Model of Autism. J Neurosci. 37:6475–6487. [PubMed: 28607173]
37. Arroyo ED, Fiole D, Mantri SS, Huang C, Portera-Cailliau C (2019): Dendritic Spines in Early Postnatal Fragile X Mice Are Insensitive to Novel Sensory Experience. J Neurosci. 39:412–419. [PubMed: 30523064]
38. Chen Q, Deister CA, Gao X, Guo B, Lynn-Jones T, Chen N, et al. (2020): Dysfunction of cortical GABAergic neurons leads to sensory hyper-reactivity in a Shank3 mouse model of ASD. Nat Neurosci. 23:520–532. [PubMed: 32123378]
39. Orefice LL, Mosko JR, Morency DT, Wells MF, Tasnim A, Mozeika SM, et al. (2019): Targeting Peripheral Somatosensory Neurons to Improve Tactile-Related Phenotypes in ASD Models. Cell. 178:867–886 e824. [PubMed: 31398341]
40. Orefice LL, Zimmerman AL, Chirila AM, Sleboda SJ, Head JP, Ginty DD (2016): Peripheral Mechanosensory Neuron Dysfunction Underlies Tactile and Behavioral Deficits in Mouse Models of ASDs. Cell. 166:299–313. [PubMed: 27293187]
41. Hisaoka T, Komori T, Kitamura T, Morikawa Y (2018): Abnormal behaviours relevant to neurodevelopmental disorders in Kirrel3-knockout mice. Sci Rep. 8:1408. [PubMed: 29362445]
42. Carvell GE, Simons DJ (1996): Abnormal tactile experience early in life disrupts active touch. J Neurosci. 16:2750–2757. [PubMed: 8786450]
43. Zhang JB, Chen L, Lv ZM, Niu XY, Shao CC, Zhang C, et al. (2016): Oxytocin is implicated in social memory deficits induced by early sensory deprivation in mice. Mol Brain. 9:98. [PubMed: 27964753]
44. Celikel T, Sakmann B (2007): Sensory integration across space and in time for decision making in the somatosensory system of rodents. Proc Natl Acad Sci U S A. 104:1395–1400. [PubMed: 17227858]
45. Kuhlman SJ, Olivas ND, Tring E, Ikrar T, Xu X, Trachtenberg JT (2013): A disinhibitory microcircuit initiates critical-period plasticity in the visual cortex. Nature. 501:543–546. [PubMed: 23975100]
46. Kang E, Durand S, LeBlanc JJ, Hensch TK, Chen C, Fagiolini M (2013): Visual acuity development and plasticity in the absence of sensory experience. J Neurosci. 33:17789–17796. [PubMed: 24198369]
47. Gianfranceschi L, Siciliano R, Walls J, Morales B, Kirkwood A, Huang ZJ, et al. (2003): Visual cortex is rescued from the effects of dark rearing by overexpression of BDNF. Proc Natl Acad Sci U S A. 100:12486–12491. [PubMed: 14514885]
48. Reh RK, Dias BG, Nelson CA 3rd, Kaufer D, Werker JF, Kolb B, et al. (2020): Critical period regulation across multiple timescales. Proc Natl Acad Sci U S A. 117:23242–23251. [PubMed: 32503914]
49. Siegel CS, Fink KL, Strittmatter SM, Cafferty WB (2015): Plasticity of intact rubral projections mediates spontaneous recovery of function after corticospinal tract injury. J Neurosci. 35:1443–1457. [PubMed: 25632122]
50. Calhoon GG, Tye KM (2015): Resolving the neural circuits of anxiety. Nat Neurosci. 18:1394–1404. [PubMed: 26404714]
51. Kim WB, Cho JH (2020): Encoding of contextual fear memory in hippocampal-amygdala circuit. Nat Commun. 11:1382. [PubMed: 32170133]
52. Cai DJ, Aharoni D, Shuman T, Shobe J, Biane J, Song W, et al. (2016): A shared neural ensemble links distinct contextual memories encoded close in time. Nature. 534:115–118. [PubMed: 27251287]

53. Pucilowska J, Vithayathil J, Pagani M, Kelly C, Karlo JC, Robol C, et al. (2018): Pharmacological Inhibition of ERK Signaling Rescues Pathophysiology and Behavioral Phenotype Associated with 16p11.2 Chromosomal Deletion in Mice. J Neurosci. 38:6640–6652. [PubMed: 29934348]

54. Garcia-Forn M, Boitnott A, Akpinar Z, De Rubeis S (2020): Linking Autism Risk Genes to Disruption of Cortical Development. Cells. 9.

55. Zahr SK, Yang G, Kazan H, Borrett MJ, Yuzwa SA, Voronova A, et al. (2018): A Translational Repression Complex in Developing Mammalian Neural Stem Cells that Regulates Neuronal Specification. Neuron. 97:520–537 e526. [PubMed: 29395907]

56. DeBoer EM, Azevedo R, Vega TA, Brodkin J, Akamatsu W, Okano H, et al. (2014): Prenatal deletion of the RNA-binding protein HuD disrupts postnatal cortical circuit maturation and behavior. J Neurosci. 34:3674–3686. [PubMed: 24599466]

57. Kraushar ML, Thompson K, Wijeratne HR, Viljetic B, Sakers K, Marson JW, et al. (2014): Temporally defined neocortical translation and polysome assembly are determined by the RNA-binding protein Hu antigen R. Proc Natl Acad Sci U S A. 111:E3815–3824. [PubMed: 25157170]

58. Kraushar ML, Viljetic B, Wijeratne HR, Thompson K, Jiao X, Pike JW, et al. (2015): Thalamic WNT3 Secretion Spatiotemporally Regulates the Neocortical Ribosome Signature and mRNA Translation to Specify Neocortical Cell Subtypes. J Neurosci. 35:10911–10926. [PubMed: 26245956]

59. Popovitchenko T, Thompson K, Viljetic B, Jiao X, Kontonyiannis DL, Kiledjian M, et al. (2016): The RNA binding protein HuR determines the differential translation of autism-associated FoxP subfamily members in the developing neocortex. Sci Rep. 6:28998. [PubMed: 27383233]

60. Popovitchenko T, Park Y, Page NF, Luo X, Krsnik Z, Liu Y, et al. (2020): Translational derepression of Elavl4 isoforms at their alternative 5′ UTRs determines neuronal development. Nature Communications. 11:1674.

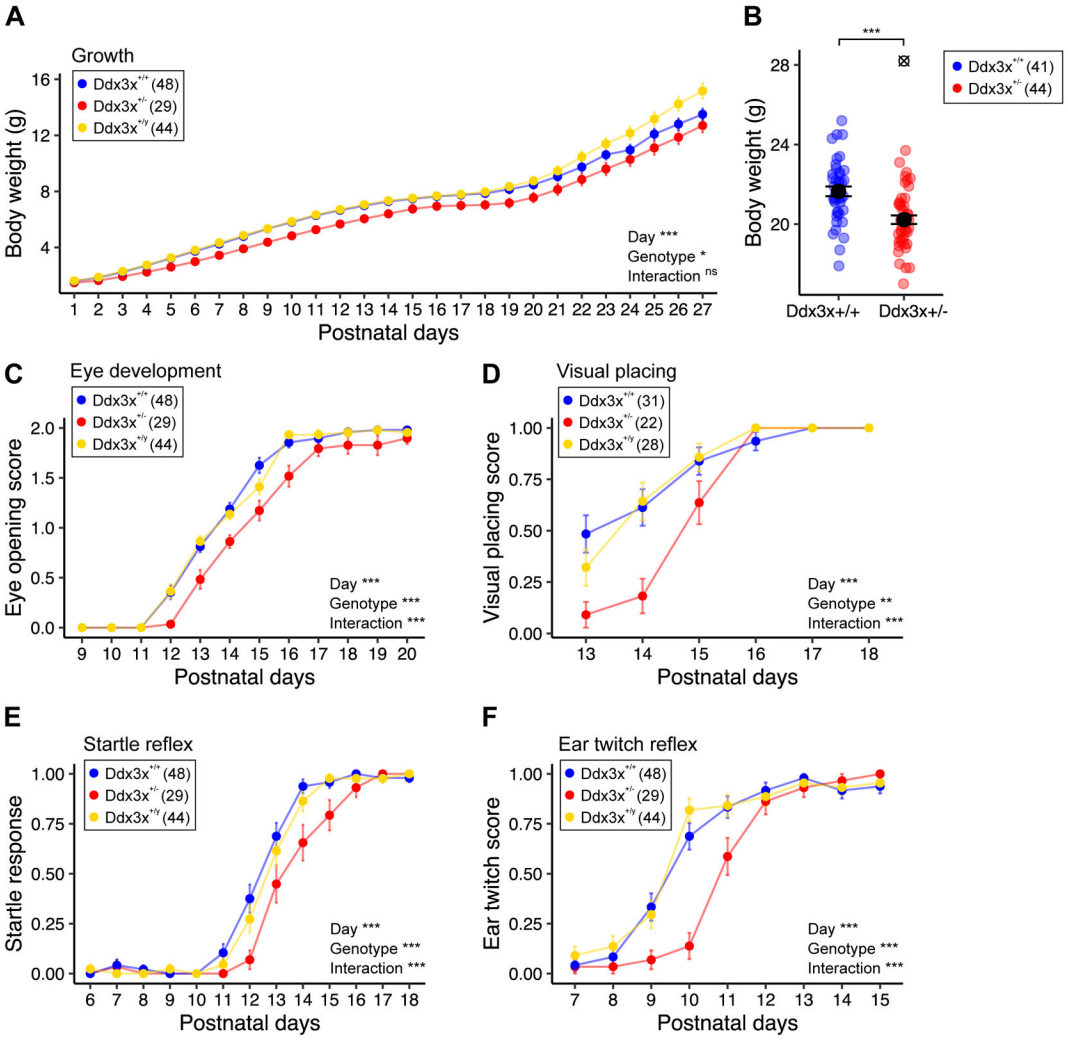

Figure 1. *Ddx3x*$^{+/-}$ mice have postnatal physical and sensory delays.

A) *Ddx3x*$^{+/-}$ pups show delayed growth. The plot shows the body weight from postnatal day (P) 1 to 27 across the three genotypes (*n* shown in legend; mean ± SEM; repeated measure ANOVA between *Ddx3x*$^{+/+}$ and *Ddx3x*$^{+/-}$ genotypes, Day: F=1055.8, df=26; Genotype: F=4.5, df=1). **B) *Ddx3x*$^{+/-}$ adults have low body weight.** The plot shows the body weight of 4-month old mice (*n* shown in legend; mean ± SEM; ⊗ indicate outliers; Student's t test after outliers removal and Shapiro-Wilk test for normality, t=4.3, df = 84). **C) *Ddx3x*$^{+/-}$ pups have a delay in eye opening.** The plot shows the eye opening scores (0, closed; 1, half-opened; 2, open) across the three genotypes (*n* shown in legend; mean ± SEM; repeated measure ANOVA between *Ddx3x*$^{+/+}$ and *Ddx3x*$^{+/-}$ genotypes; Day: F=593, df=11; Genotype: F=18, df=1; Interaction: F=5, df=11). **D) *Ddx3x*$^{+/-}$ pups show a delay in developing visual placing skills.** The plot shows the visual placing scores (0, response absent; 1, response present) across the three genotypes. Visual response was considered present (score 1) when pups lowered onto a flat surface reached out with the forepaws before the vibrissae touched the surface (*n* shown in legend; mean ± SEM; repeated measure ANOVA between *Ddx3x*$^{+/+}$ and *Ddx3x*$^{+/-}$ genotypes; Day: F=53.8, df=5;

Genotype: F=11.8, df=1; Interaction: F=6.6, df=5). **E) *Ddx3x*$^{+/-}$ pups have a delay in developing a startle response to an auditory cue.** The plot shows the startle response score (0, response absent; 1, response present) across the three genotypes. Startle response was considered present (score 1) when pups turned their heads in response to an 80db click sound (*n* shown in legend; mean ± SEM; repeated measure ANOVA between *Ddx3x*$^{+/+}$ and *Ddx3x*$^{+/-}$ genotypes; Day: F=285.2, df=12; Genotype: F=12.7, df=1; Interaction: F=4.9, df=12). **F) *Ddx3x*$^{+/-}$ pups show a delay in developing an ear twitch response to a tactile stimulus.** The plot shows the reflex to ear twitch response (0, response absent; 1, response present) across the three genotypes (*n* shown in legend; mean ± SEM; repeated measure ANOVA between *Ddx3x*$^{+/+}$ and *Ddx3x*$^{+/-}$ genotypes; Day: F=142.6, df=8; Genotype: F=12.2, df=1; Interaction: F=8.5, df=8). All data collected and scored blind to genotype. In all panels, *Ddx3x*$^{+/+}$ (blue), *Ddx3x*$^{+/-}$ (red), and *Ddx3x*$^{+/y}$ (yellow). *p<0.05, **p<0.01, ***p<0.001; ns, non significant.

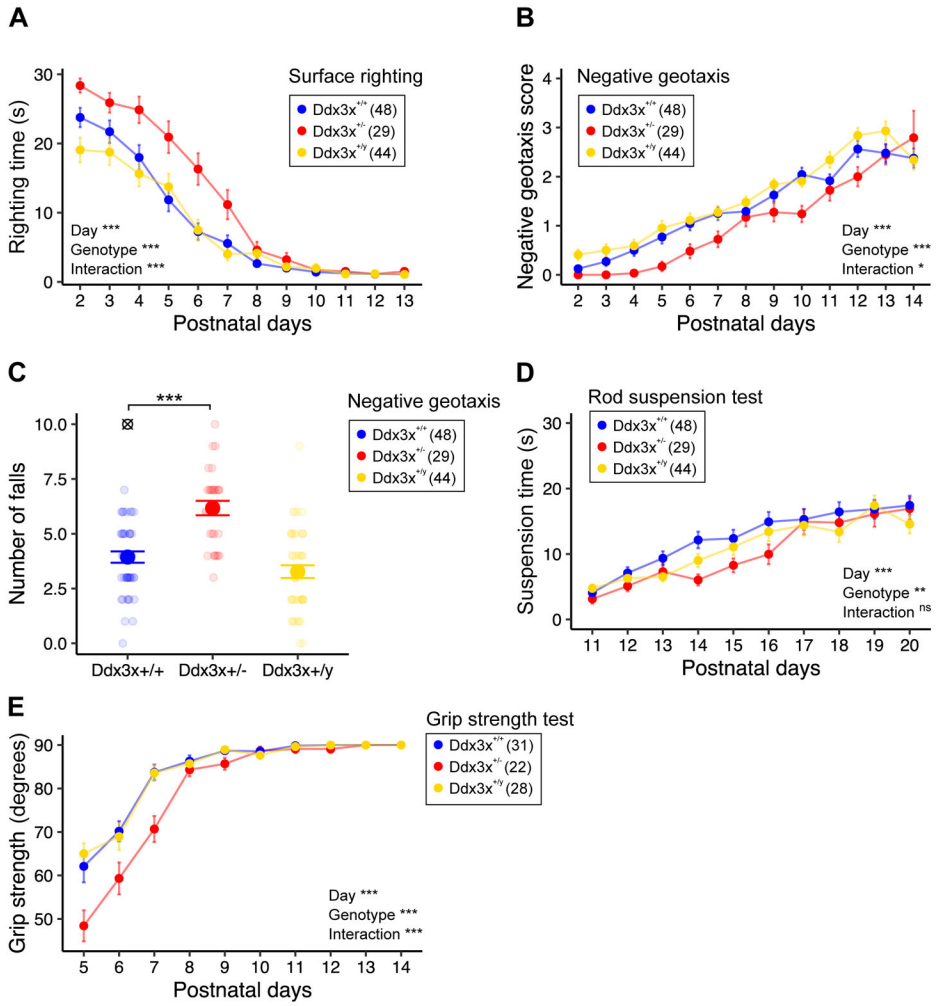

Figure 2. *Ddx3x*$^{+/-}$ mice have postnatal motor delays.

A) *Ddx3x*$^{+/-}$ pups have a delay in surface righting time. The plot shows the time that it takes for a pup to turn on the four paws from a supine position across the three genotypes (*n* shown in legend; mean ± SEM; repeated measure ANOVA between *Ddx3x*$^{+/+}$ and *Ddx3x*$^{+/-}$ genotypes; Day: F=131.1, df=11; Genotype: F=24.7, df=1; Interaction: F=4.1, df=11). **B) *Ddx3x*$^{+/-}$ pups have a delay in acquiring negative geotaxis skills.** The plot shows the response of the pup when placed head down on a mesh covered platform at a 45° angle (0, fall; 1, stay/move down/walk down; 2, turn and stay; 3, turn, move up, and stay; 4, turn and move up to the top) across the three genotypes (*n* shown in legend; mean ± SEM; repeated measure ANOVA between *Ddx3x*$^{+/+}$ and *Ddx3x*$^{+/-}$ genotypes; Day: F=57.5, df=12; Genotype: F=16.1, df=1; Interaction: F=1.8, df=12). **C) *Ddx3x*$^{+/-}$ pups tend to fall more in a negative geotaxis task.** The plot shows the number of falls (score 0) per pup across the three genotypes (*n* shown in legend; mean ± SEM; ⊗ indicate outliers; Student's t test after outliers removal and Shapiro-Wilk test for normality; t=6, df=74). **D) *Ddx3x*$^{+/-}$ pups have reduced motor endurance and performance in a rod suspension test.** The plot shows the time that it takes for a pup to fall off a rod across the three genotypes (*n* shown in legend; mean ± SEM; repeated measure ANOVA between *Ddx3x*$^{+/+}$ and *Ddx3x*$^{+/-}$ genotypes; Day:

F=29.4, df=9; Genotype: F=4.4, df=1; Interaction: F=1.3, df=9). **E) *Ddx3x*$^{+/-}$ pups have reduced grip strength.** Grip strength was tested by placing pups on a mesh grid and rotating the grid from a horizontal to vertical position. The plot shows the angle of rotation to which pups fall off the grid across the three genotypes (*n* shown in legend; mean ± SEM; repeated measure ANOVA between *Ddx3x*$^{+/+}$ and *Ddx3x*$^{+/-}$ genotypes; Day: F=94.5, df=9; Genotype: F=17.9, df=1; Interaction: F=5.4, df=9). All data collected and scored blind to genotype. In all panels, *Ddx3x*$^{+/+}$ (blue), *Ddx3x*$^{+/-}$ (red), and *Ddx3x*$^{+/y}$ (yellow). *p<0.05, **p<0.01, ***p<0.001; ns, non significant.

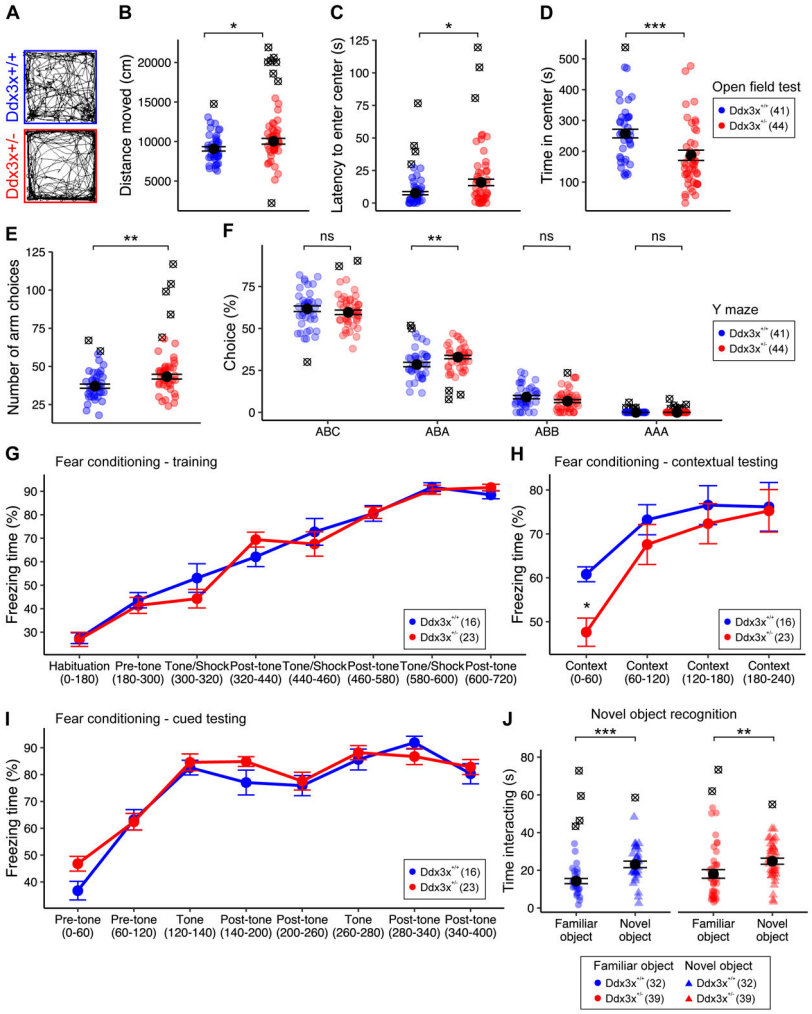

Figure 3. *Ddx3x*$^{+/-}$ mice have hyperactivity, anxiety-like behaviors, and cognitive deficits.

A-B) *Ddx3x*$^{+/-}$ mice show increased locomotor activity in open field test. Panel A shows an example of activity of individual mice in a 10-min interval. The plot in B shows the distance covered in the 30-min open field test (*n* shown in legend; mean ± SEM; Student's t test, t=2.1, df = 76). **C) *Ddx3x*$^{+/-}$ mice display increased latency to enter the center zone.** The plot shows the latency to enter the center zone for the two genotypes (*n* shown in legend; mean ± SEM; Wilcoxon signed-rank test, W=567). **D) *Ddx3x*$^{+/-}$ mice have increased thigmotaxis.** The plot shows the time spent in the center zone for the two genotypes (*n* shown in legend; mean ± SEM; Wilcoxon signed-rank test, W=1327). **E) *Ddx3x*$^{+/-}$ mice have increased activity in Y maze spontaneous alternation test.** The plot shows the number of arms explored in a 15-min test for the two genotypes (*n* shown in legend; mean ± SEM; Student's t test, t=2.9, df = 77). **F) Short-term working memory is overall intact in *Ddx3x*$^{+/-}$ mice in Y maze spontaneous alternation test.** The plot shows the percentage of choices, broken down by choice type. 'ABC' indicates correct alternations, while 'ABA', 'ABB', 'AAA' errors (*n* shown in legend; mean ± SEM; ABA choice: Student's t test, t=2.7, df=79). **G) *Ddx3x*$^{+/-}$ mice have no alterations in fear conditioning training.** The plot shows the percentage of time spent freezing during training

(*n* shown in legend). **H) *Ddx3x*$^{+/-}$ mice display weaker initial recall of contextual fear memory.** After 24 hours from contextual and cued training (**G**), mice were exposed to the same environment of training, but without the administration of tones or shocks, for 240 sec. The plot shows the % of time the mice spent freezing during this 240 sec testing trial (*n* shown in legend; mean ± SEM; repeated measure ANOVA over the first 120 sec, Genotype: F=4.9, df=1). **I) *Ddx3x*$^{+/-}$ mice show no changes in cued fear memory.** After 24 hrs from contextual testing (**H**), mice were exposed to a new environment, with administration of two tones without subsequent shock exposure. The plot shows the % of time the animals spent freezing during this 400 sec testing trial. **J) *Ddx3x*$^{+/-}$ mice spend more time with a novel object than a familiar one, as their control littermates.** The plot shows the time mice spent interacting a novel object (triangles) or a familiar object (circles) during a 5 min testing session (*n* shown in legend; mean ± SEM; *Ddx3x*$^{+/+}$: Student's t test, t=3.9, df=57; *Ddx3x*$^{+/-}$: Wilcoxon signed-rank test, W=436). All data collected and scored blind to genotype. For all tests, statistical testing was conducted after removing outliers (indicated as ⊗) assessing normality with the Shapiro-Wilk test. In all panels, *Ddx3x*$^{+/+}$ (blue) and *Ddx3x*$^{+/-}$ (red). *p<0.05, **p<0.01, ***p<0.001; ns, non significant.

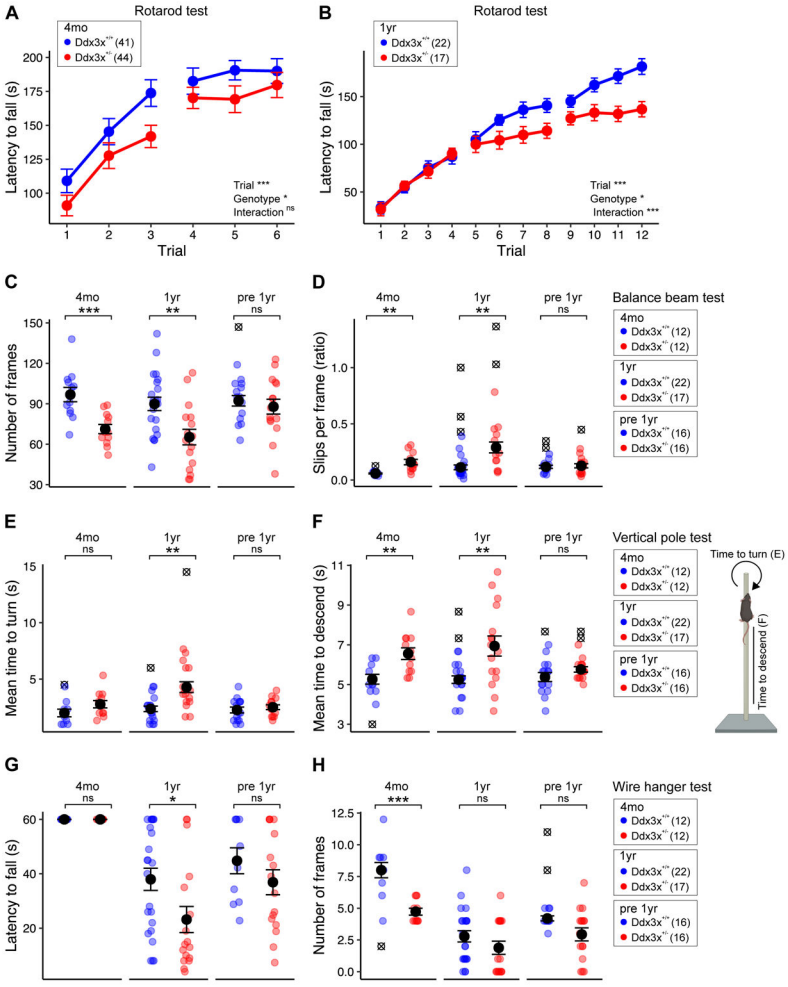

Figure 4. *Ddx3x*$^{+/-}$ mice have motor deficits, which attenuate in ageing mice previously exposed to behavioral training.

A) Adult *Ddx3x*$^{+/-}$ mice have suboptimal motor performance on a rotarod test. Trials were conducted one hour apart with an acceleration over 5 minutes, and trials 1-3 were performed 24 hrs before trials 4-6, to assess both short-term (1 hour) and long-term (24 hrs) motor learning on 4-month old mice (4mo). The plot shows the latency to fall from the rod (*n* shown in legend; mean ± SEM; repeated measure ANOVA; Trial: F=52.9, df=5; Genotype: F=4.1, df=1; Interaction: F=0.79, df=5). **B) Ageing *Ddx3x*$^{+/-}$ mice have altered motor learning on a rotarod test.** Trials were conducted one-hour apart with an acceleration over 5 min, with trials 1-4, 5-8 and 9-12 performed 24 hrs apart on one-year old mice (1 yr). The plot shows the latency to fall from the rod (*n* shown in legend; mean ± SEM; repeated measure ANOVA; Trial: F=125.1, df=11; Genotype: F=5.2, df=1; Interaction: F=4.8, df=11). **C-D) Adult and ageing *Ddx3x*$^{+/-}$ mice have impaired motor coordination in the balance beam test, but these changes are not observed in ageing mice previously exposed to behavioral training (pre 1yr).** Panel C shows the number of frames covered (*n* shown in legend in panel D; mean ± SEM; 4mo: Welch's t-test, t=4.04, df=22; 1yr: Welch's t-test, t=3.24, df=37; pre 1yr: Welch's t-test, t=0.6, df=29). Panel D shows the number of slips per frame (*n* shown in legend; mean ± SEM; 4mo: Welch's

t-test, t=4.13, df=11.7; 1yr: Wilcoxon signed-rank test, W=45.5). **E) Ageing *Ddx3x*$^{+/-}$ mice have age-dependent deficits in turning in the vertical pole test, but these changes are prevented by prior behavioral training (pre 1yr).** The plot shows the mean time to turn on the top of the vertical pole (*n* shown in legend in panel F; mean ± SEM; 1yr: Welch's t-test, t=3.6, df=22.6). **F) Adult and ageing *Ddx3x*$^{+/-}$ mice have altered balance during the vertical pole test, but these changes are not observed in ageing mice previously exposed to behavioral training (pre 1yr).** The plot shows the mean time to descend the vertical pole (*n* shown in legend; mean ± SEM; 4mo: Student's t test, t=3.3, df=20; 1yr: Welch's t-test, t=3.1, df=19.2). **G) *Ddx3x*$^{+/-}$ mice have age-dependent changes in endurance in the wire hanging test.** The plot shows the latency to fall (*n* shown in legend in panel H; mean ± SEM; 1yr: Wilcoxon signed-rank test, W=280). **H) *Ddx3x*$^{+/-}$ mice show changes in motor ability in the wire hanging test.** The plot shows the number of frames covered by the mice (*n* shown in legend; mean ± SEM; 4mo: Wilcoxon signed-rank test, W=112). All data collected and scored blind to genotype. For all tests, statistical testing was conducted after removing outliers (indicated as ⊗) and assessing normality with the Shapiro-Wilk test. In all panels, *Ddx3x*$^{+/+}$ (blue) and *Ddx3x*$^{+/-}$ (red). *p<0.05, **p<0.01, ***p<0.001; ns, non significant.

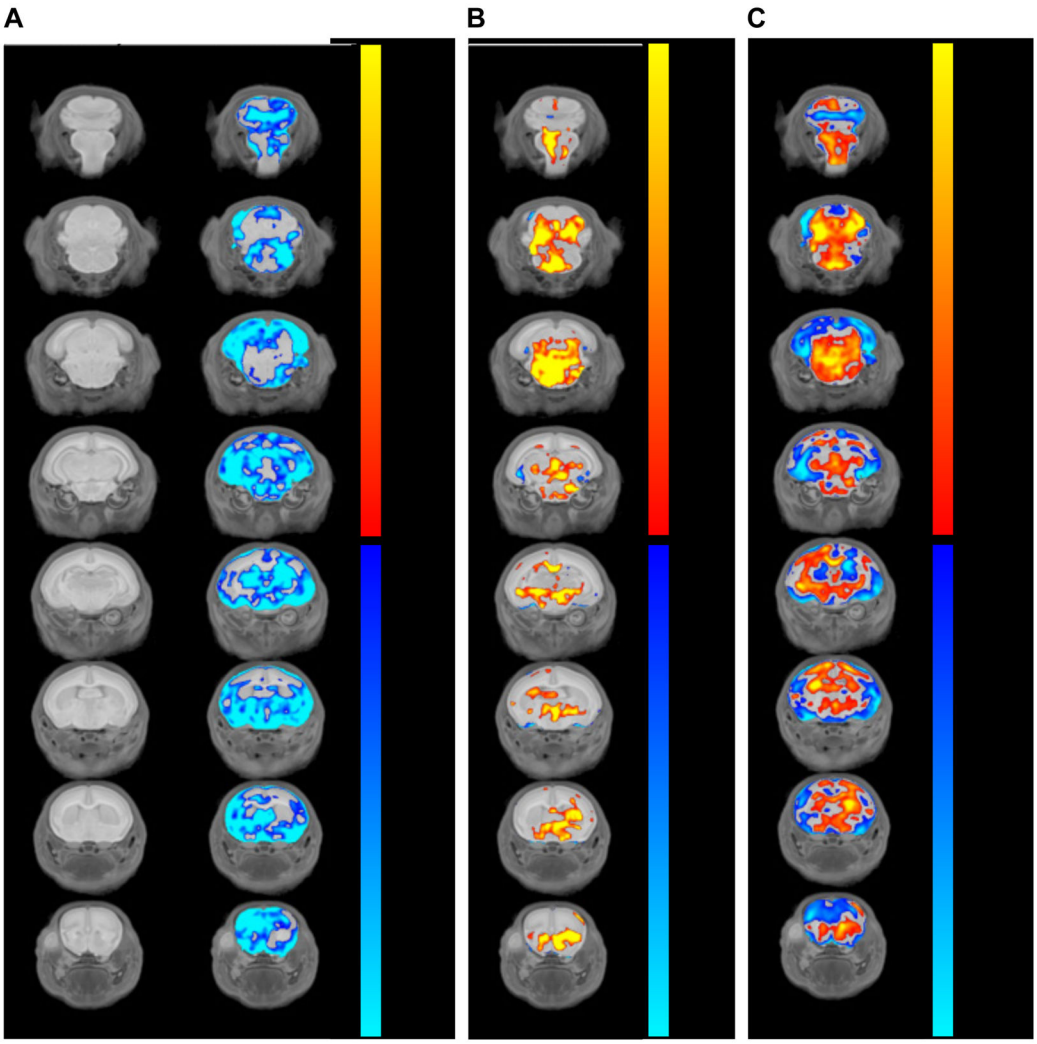

Figure 5. *Ddx3x*$^{+/-}$ mice have voxelwise differences in brain volume.

A) *Ddx3x*$^{+/-}$ pups have reduced brain volume. Coronal flythrough from anterior (top row) to posterior (bottom row), showing brain anatomy (left column) and absolute differences in *Ddx3x*$^{+/-}$ vs *Ddx3x*$^{+/+}$ mice (right column) at P3. The color coding indicates the false discovery rate (FDR) for regions that are smaller (blue gradient) or larger (red gradient) in *Ddx3x*$^{+/-}$ compared to *Ddx3x*$^{+/+}$ mice (n=10/genotype). **B) Changes in relative brain volume in *Ddx3x*$^{+/-}$ pups.** Same as in A, showing voxelwise changes relative to the overall reduction in brain volume (n=10/genotype). **C) Specific brain regions are disproportionally reduced in *Ddx3x*$^{+/-}$ pups.** Same as in A, with the color coding indicating the percentage of difference between *Ddx3x*$^{+/-}$ and *Ddx3x*$^{+/+}$ mice for regions that are disproportionally smaller (blue gradient) or larger (red gradient) that the ~10% reduction in overall brain volume (n=10/genotype). All data used to generate these plots, include individual-level data, are reported in Table S4. All data collected and analyzed blind to genotype.

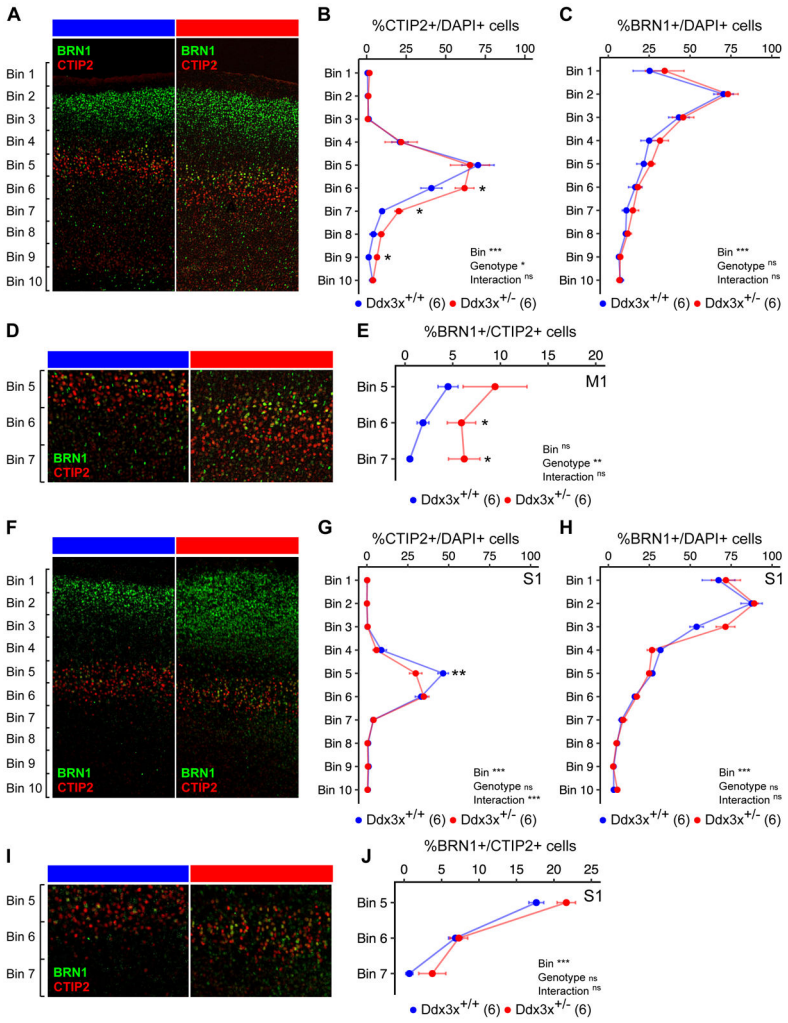

Figure 6. *Ddx3x*$^{+/-}$ mice have altered cortical lamination.

A) *Ddx3x*$^{+/-}$ mice show a misplacement of ScPN projection neurons in the developing cortex. Representative confocal images of coronal sections of primary motor cortex (M1) from *Ddx3x*$^{+/+}$ and *Ddx3x*$^{+/-}$ mice at P3, immunostained for CTIP2 (red), a marker of ScPN and BRN1 (green), a marker of IT in UL and DL. As expected, CTIP2+ ScPN are restricted to layer V, while BRN1+ IT are predominantly in upper layers in control mice. **B) CTIP2+ ScPN extend deeper in *Ddx3x*$^{+/-}$ mice in the primary motor cortex.** Distribution of the percentage of cells (DAPI+) that are positive to the ScPN marker CTIP2, across ten equally sized bins from the pia (bin 1) to the ventricle (bin 10) in *Ddx3x*$^{+/+}$ and *Ddx3x*$^{+/-}$ mice (*n* shown in legend; 6-8 sections/mouse, with outliers across sections removed; mean ± SEM; Two-way ANOVA: Genotype: F=4, df=1; Bins: F=43.3, df=9; Bin 6: Student's t test, t=2.3, df=10; Bin 7: Welch Two Sample t-test, t=4.3, df=4.1; Bin 9: Wilcoxon signed-rank test, W=2). **C) BRN1+ IT neurons appear grossly normal in the motor cortex of *Ddx3x*$^{+/-}$ mice.** Distribution of the percentage of cells (DAPI+) that are positive to the IT marker BRN1, across ten equally sized bins from the pia (bin 1) to the ventricle (bin 10) in *Ddx3x*$^{+/+}$ and *Ddx3x*$^{+/-}$ mice (*n* shown in legend; 6-8 sections/mouse, with outliers across sections removed; mean ± SEM; Two-way ANOVA: Bin: F=28.2, df=9). **D) CTIP2+ and**

BRN1+ are mostly mutually exclusive, but not in *Ddx3x*$^{+/-}$ mice. The panels show a magnification of the bins 5-7 regions from panel A. As expected, in control mice, a minority of CTIP2+ neurons is positive to BRN1. **E) In *Ddx3x*$^{+/-}$ mice, there are more CTIP2+BRN1+ neurons in deep layers.** Distribution of the percentage of CTIP2+ ScPN that are also positive to BRN1, across bins 5-7, where CTIP2+ ScPN are most abundant (*n* shown in legend; 6-8 sections/mouse, with outliers across sections removed; mean ± SEM; Two-way ANOVA: Genotype: F=11, df=1; Bin 6: Student's t test, t=2.5, df=10). **F)**. Same as A, but from the primary somatosensory cortex (S1). **G) There is an excess of CTIP2+ ScPN in *Ddx3x*$^{+/-}$ mice in the primary somatosensory cortex.** Same as B, but on S1. (*n* shown in legend; 6-8 sections/mouse, with outliers across sections removed; mean ± SEM; Two-way ANOVA: Bin: F=119.5, df=9; Interaction: F=3.9, df=9; Bin 5: Student's t test, t=3.3, df=9). **H) BRN1+ IT neurons appear grossly normal in the somatosensory cortex of *Ddx3x*$^{+/-}$ mice.** Same as C, but on the somatosensory cortex. (*n* shown in legend; 6-8 sections/mouse, with outliers across sections removed; mean ± SEM; Two-way ANOVA: Bin: F=108.2, df=9). **I) CTIP2+BRN1+ neurons in S1.** The panels show a magnification of the bins 5-7 regions from panel I. **J) No changes in CTIP2+BRN1+ neurons in S1.** Distribution of the percentage of CTIP2+ neurons that are also positive to BRN1, across bins 5-7, where CTIP2+ ScPN are most abundant (*n* shown in legend; 6-8 sections/mouse, with outliers across sections removed; mean ± SEM; Two-way ANOVA: Bin: F=99.8, df=2). In all panels, scale bar corresponds to 120 μm. All data collected and scored blind to genotype. For all tests, statistical testing was conducted after removing outliers and assessing normality with the Shapiro-Wilk test. In all panels, *Ddx3x*$^{+/+}$ (blue) and *Ddx3x*$^{+/-}$ (red). *p<0.05, **p<0.01, ***p<0.001; ns, non significant.

KEY RESOURCES TABLE

Resource Type	Specific Reagent or Resource	Source or Reference	Identifiers	Additional Information
Add additional rows as needed for each resource type	Include species and sex when applicable.	Include name of manufacturer, company, repository, individual, or research lab. Include PMID or DOI for references; use “this paper” if new.	Include catalog numbers, stock numbers, database IDs or accession numbers, and/or RRIDs. RRIDs are highly encouraged; search for RRIDs at https://scicrunch.org/resources.	Include any additional information or notes if necessary.
Antibody	Anti-DDX3X, rabbit polyclonal	Millipore	#09-860	
Antibody	Anti-GAPDH, mouse monoclonal	Millipore	#CB1001	
Antibody	Anti-SATB2, rabbit monoclonal	Abcam	#ab51502	
Antibody	Anti-CTIP2/BCL11B, rat monoclonal	Millipore	#MABE1045	
Antibody	anti-BRN1/POU3F3, goat polyclonal	Novus Biologicals	#NBP1-49872	
Antibody	anti-PKA C-α, rabbit polyclonal	Cell Signaling	#4782	
Antibody	anti-VGLUT1, rabbit polyclonal	Synaptic Systems	#135-302	
Antibody	anti-PSD95, mouse monoclonal	NeuroMab	#75-028	
Antibody	anti-TBR1, rabbit polyclonal	Abcam	#ab51502	
Antibody	anti-LMO4, rat monoclonal	Millipore	#MABN2274	
Antibody	anti-BHLHB5, guinea pig	gift from Dr. Novitch's lab	n/a	
Chemical Compound or Drug	TRIzol™ LS Reagent	Invitrogen	#10296010	
Commercial Assay Or Kit	High Capacity cDNA Reverse Transcription Kit	AppliedBiosystems	#4368813	
Commercial Assay Or Kit	TaqMan™ Fast Advanced Master Mix	AppliedBiosystems	#4444556	
Commercial Assay Or Kit	TaqMan™ Gene Expression Assays - DDX3X	AppliedBiosystems	#Mm00657923_g1	
Commercial Assay Or Kit	TaqMan™ Gene Expression Assays - GAPDH	AppliedBiosystems	#Mm99999915_g1	
Chemical Compound or Drug	Percoll™ Plus	Sigma-Aldrich	#P1644	
Chemical Compound or Drug	SDS gels: 4–20% Mini-PROTEAN® TGX Stain-Free™ Protein Gels	Bio-Rad	#4568094	
Chemical Compound or Drug	RIPA Lysis and Extraction Buffer	ThermoFisher	#89901	
Chemical Compound or Drug	RNasin™ ribonuclease inhibitors	ThermoFisher	#N8080119	
Commercial Assay Or Kit	Pierce™ BCA Protein Assay Kit	ThermoFisher	#23225	
Organism/Strain	*Ddx3x*^{flox}	This paper (generated at Ozgene)	n/a	

Resource Type	Specific Reagent or Resource	Source or Reference	Identifiers	Additional Information
Organism/Strain	*Ddx3x*$^{flox/+}$;Sox2-Cre/+ females	This paper	n/a	
Organism/Strain	B6.Cg-Edil3$^{Tg(Sox2-cre)1Amc}$/J	The Jackson Laboratory	#008454	
Oligonucleotides	Primer 4539 for genotype of wild type (*Ddx3x*$^{+}$), floxed (*Ddx3x*^{flox}), or Δexon2 (*Ddx3x*$^{-}$) alleles (forward): 5'-GATGCATACAACATCCTGAACC-3'	Custom designed, synthesized at ThermoFisher	n/a	
Oligonucleotides	Primer 4540 for genotype of wild type (*Ddx3x*$^{+}$), floxed (*Ddx3x*^{flox}), or Δexon2 (*Ddx3x*$^{-}$) alleles (reverse): 5'-GCCCTGACTTCAAACCTCTTAG-3'	Custom designed, synthesized at ThermoFisher	n/a	
Oligonucleotides	Primer 4541 for genotype of *Ddx3x*$^{+}$ or *Ddx3x*^{flox} (reverse): 5'-CTTGCTGTACTTCCTCCACTCTG-3'	Custom designed, synthesized at ThermoFisher	n/a	
Oligonucleotides	Primer 4572 for detection of the *Cre* transgene (forward): 5'-AATGGTTTCCCGCAGAACCT-3'	Custom designed, synthesized at ThermoFisher	n/a	
Oligonucleotides	Primer 4573 for detection of the *Cre* transgene (reverse): 5'-GCATTGCTGTCACTTGGTCG-3'	Custom designed, synthesized at ThermoFisher	n/a	
Oligonucleotides	Primer 4598 for detection of the *Sry* gene (forward): 5'-TGGCAGCCTGTTGATATCCC-3'	Custom designed, synthesized at ThermoFisher	n/a	
Oligonucleotides	Primer 4599 for detection of the *Sry* gene (reverse): 5'-CTGAGGTGCTCCTGGTATGG-3'	Custom designed, synthesized at ThermoFisher	n/a	
Software; Algorithm	Noldus EthoVision	Noldus	v11.4	
Software; Algorithm	RStudio Version 1.2.5042	RStudio	https://rstudio.com	
Software; Algorithm	ImageJ	Schneider et al., 2012	https://imagej.nih.gov/ij/	
Software; Algorithm	GIMP	GIMP Team	https://www.gimp.org	